EXAFS studies of molten $ZnCl_2$, RbCl and Rb_2ZnCl_4

1994 J. Phys.: Condens. Matter 6 3629

(http://iopscience.iop.org/0953-8984/6/20/003)

J. Phys.: Condens. Matter 6 (1994) 3629–3640. Printed in the UK

EXAFS studies of molten $ZnCl_2$, RbCl and Rb_2ZnCl_4

Li Hefeng, Lu Kunquan, Wu Zhonghua and Dong Jun

Institute of Physics, Chinese Academy of Sciences, Beijing 100080, People's Republic of China

Received 17 December 1993, in final form 22 February 1994

Abstract. The local structures of molten $ZnCl_2$, RbCl and Rb_2ZnCl_4 are measured with the EXAFS technique. Several models are used to analyse the data, and some structural parameters as well as the radial distribution functions of the nearest-neighbour atoms around Zn or Rb atoms are obtained. The tetrahedra consisting of four Cl atoms around Zn are found to be dominant and stable in molten $ZnCl_2$. The skewed behaviour of the radial distribution function for Rb–Cl in molten RbCl is also found, while the local structures around Rb can be regarded as a persistence of the solid state but with strong short-range disorder. In molten Rb_2ZnCl_4, a network linked by Zn Cl_4 groups is not found and the nearest-neighbour structures around Rb atoms are more disordered than in molten RbCl. This has also confirmed that the EXAFS method can provide reliable information about the nearest-neighbour atom–atom coordination for some molten salts, which is helpful in specifying the pairwise interaction potential.

1. Introduction

The structures of some molten salts have been studied using various methods over the past decades. The three partial distribution functions in molten $ZnCl_2$ were obtained from x-ray [1] and neutron diffraction [2]. Molecular dynamics simulations [3–5] also provided a successful description of the melt. According to those studies, the melt consists of a closely packed Cl^- structure in which Zn^{2+} ions reside in tetrahedrally coordinated sites and the distribution functions show almost no penetration of like ions in the nearest-neighbour shell. Allen *et al* [6] studied the structure of $ZnCl_2$ in the liquid state with pulsed neutron diffraction. Considering the character of the total distribution function $G(r)$, they confirmed that the tetrahedral unit is both well defined and long lived in the melt, which is more usually associated with covalently bonded liquids, and is in agreement with the result that little diffusion is taking place in $ZnCl_2$ at a temperature just above the melting point. Wong and Lytle [7] also measured the local structure around Zn in the melt with the EXAFS technique, which yielded somewhat larger values for the Zn–Cl distance and coordination number than the previous result.

The three partial pair distribution functions of RbCl just above its melting point have been determined by applying the technique of neutron scattering to isotopically doped samples [8]. The first peak of the anion–cation distribution function $g_{+-}(r)$ is asymmetrically broadened and a small amount of penetration is evident by comparing the function $g_{+-}(r)$ with $g_{++}(r)$. The peak position of $g_{+-}(r)$ and the coordination number for the unlike ions are 3.18 Å and 6.9, respectively. The experimentally determined distribution functions are in good agreement with those taken from molecular dynamics simulation using the rigid ion and polarizable ion models completed by Dixon and Sangster [9]. In addition, the structures of molten $ZnCl_2$ + LiCl and $ZnCl_2$ + KCl mixtures were investigated with

0953-8984/94/203629+12$19.50

Raman scattering [10] and pulsed neutron diffraction [11] separately. Allen *et al* [11] found that the tetrahedral structures of Zn–4Cl are stable as in molten $ZnCl_2$ and not readily perturbed by the addition of another chloride, but the structure of KCl is greatly modified even by adding a few per cent of $ZnCl_2$.

The mechanism of successive phase transitions in Rb_2ZnCl_4 has aroused a great deal of interest; the properties and structure of this compound have been widely studied [12–15]. At room temperature, Rb_2ZnCl_4 is paraelectric and has four formula units in an orthorhombic cell (space group *Pnam*). It is highly disordered because the four Cl atoms are scattered around Zn at three distances from 2.233 Å to 2.254 Å and Rb atoms occupy two inequivalent positions, in which there are 8Cl (with five distances from 3.261 Å to 3.727 Å) for Rb(1)–Cl and 9Cl (with six distances from 3.312 Å to 3.861 Å) for Rb(2)–Cl [12]. Furthermore, on increasing temperature from 303 K to 600 K, every $ZnCl_4$ group liberates between two possible orientations, which can enhance the disordered motions of the neighbouring Rb atoms [13, 14]. Since no structural data have been reported on molten $Rb_2ZnCl-4$, an interesting question is, what is its local structure in the liquid state?

In this paper we make an attempt to find out whether the local structures of Rb_2ZnCl_4 in the solid state are still retained in its liquid state or whether the melt is separated into structures similar to those in molten $ZnCl_2$ and RbCl respectively. The results are not only useful for recognizing the character and origin of the interatomic interactions but also very significant for explaining the phenomenon of melting and the mechanisms of crystal growth, for example, to discover whether the large static disorder around Rb–Cl in the solid Rb_2ZnCl_4 has its origins in the melt.

In our work, the nearest-neighbour coordination structures around Zn and Rb in $ZnCl_2$, RbCl and Rb_2ZnCl_4 melts are obtained using the EXAFS method. The EXAFS technique is a powerful tool for measuring the structure of dissolved systems, such as non-crystals, glasses and liquids in which the long- and even medium-range order is lost. With a suitable reference, the *r*-space resolution of EXAFS can be better than that achieved with most conventional diffraction methods. The characteristic of gaining local structural information around the particular type of absorption atom, as well as the backscattering amplitude and the phase-shift being very sensitive to the types of backscattering atom, enable it to directly provide the coordination of interest more conveniently than the neutron diffraction substitution method. In addition, because the EXAFS method has the ability to determine the radial distribution function (RDF) with accuracy, the atom–atom pair correlation function can then be obtained, which is valuable for searching for a suitable model for the pairwise interaction potential in a molecular dynamics calculation [16]. The conventional data analysis procedure with the Gaussian approximation is no correct for large disordered systems. Some new data analysis methods have been established [17–20]. The advantages and limitations of these methods are discussed in [18] and [21].

For a system with large disorder, the cumulant expansion method [17, 18] is inappropriate and the procedure of fitting experimental data with assumed models should be adopted. In order to overcome some shortcomings of the model-dependent method, in our work different models are used and compared with caution to find the most competent one.

In section 2, the sample preparation and the experimental measurement are briefly described. The details of the data analysis procedure are given in section 3 and finally the discussion and conclusions are in section 4.

2. Experimental details

Anhydrous $ZnCl_2$, crystalline powder RbCl and single-crystal Rb_2ZnCl_4 were each sufficiently ground into enough fine powder. Then the appropriate weight of each was well mixed with exactly the right amount of powdered BN, which is a suitable material as a support because of its high melting point and high temperature stability as well as low x-ray absorption. Here BN powder was obtained from an alcohol suspension to obtain small enough particles to ensure that the mixture was sufficiently homogeneous. The appropriate composition of each mixture was calculated according to the densities and absorption coefficients of the compounds involved for the appropriate thickness of a sample to satisfy $\mu x \leqslant 1.5$, $\Delta\mu x \leqslant 1.0$ where possible; here μx and $\Delta\mu x$ are the total absorption and the absorption step just above the edge of a particular atom. All the preparations above were performed in a large dry box filled with He gas and then the EXAFS samples were obtained by swiftly pressing the mixture using a pressure machine to form discs with appropriate thicknesses.

Each sample was heated to above its melting point (T_m) for 1 h and then cooled down to room temperature. Both the heated and unheated samples were examined by x-ray diffraction to identify that the reaction between the compound of interest and BN had not taken place even at high temperature.

Most of the EXAFS measurements were carried out on the beam lines 10B and 7C at the synchrotron radiation source of the Photon Factory in Japan using an Si(311) channel-cut monochromator (BL-10B) and a Si(111) double-crystal one (BL-7C); the ring current is about 150–300 mA at 2.5 GeV. The detector system consisted of two ionization chambers filled with a mixture of Ar and N_2. Higher harmonics were eliminated by detuning at BL-7C, while at BL-10B they were kept as small as possible by choosing appropriate lengths of the two ionization chambers and an appropriate ratio of the two kinds of gas. the Cu K edge (8980.3 eV) was used to calibrate the energy scale. For each absorption edge, several experimental scans were recorded in order to estimate the statistical errors of the results.

The EXAFS of Zn K edges for $ZnCl_2$ samples were measured at 300 K and 613 K (T_m = 591 K) and those for Rb_2ZnCl_4 at 823 K (T_m = 793 K). The EXAFS of Rb K edges for RbCl samples were measured at 1023 K (T_m = 988 K), and those for Rb_2ZnCl_4 at 823 K. All the measurements were taken in the transmission mode.

The EXAFS data of Rb K edge at 80 K were collected at the beam line 4W1B at Beijing Synchrotron Radiation Facility. The storage ring was running at 2.2 GeV and the current was about 30 mA. The higher-harmonic elimination and the detector system were the same as those at BL-7C of the Photon Factory. The sample was made by rubbing sufficiently fine RbCl powder onto Scotch tape and several layers were used to achieve a satisfactory thickness. The sample was then set in a refrigerator.

For the measurements at high temperatures, the samples were heated in a water-cooled furnace, which was filled with flowing He gas to maintain an appropriate positive pressure inside in order to protect the sample against oxidization. The temperature was controlled and monitored using a temperature controller model 818P with an accuracy better than ±1 °C. The EXAFS measurement started when the sample had been sufficiently melted about 20 min. The decrease in $\Delta\mu x$ was small for each molten sample relative to that of the solid state; while the absorption spectrum of the resolidified sample was compared with that of the unheated one, only a subtle change was found. These findings indicated that no serious leakage or oxidization occurred during the measurements.

3. Data analysis

All the experimental data at high temperatures have been fitted using several types of model function in our work. These are as follows.

(i) *Two-Gaussian-subshell model (MD1).* Assuming the nearest-neighbour distribution is composed to two Gaussian subshells, then the isolated EXAFS functions can be written as

$$\chi(k) = \sum_{i=1}^{2} \frac{N_i}{\bar{r}_i^2} B(k) \mathrm{e}^{-2k^2\sigma_i^2} \sin\left[2k\bar{r}_i + \delta(k)\right] \tag{1}$$

where $B(k) = S_0^2(k)F_i(k)\mathrm{e}^{-2r_i/\lambda}$. The structure parameters N_i and $\bar{r}_i$ can be obtained with the conventional fitting procedure, then the normalized RDF is easily constructed.

(ii) *Skewed exponential model [17, 18] (MD2).* This kind of model is suitable for the presence of larger asymmetrical distributions. The normalized effective RDF is

$$\begin{aligned} P^m(r) &= \left\{\left[\mathrm{e}^{-2(r-\bar{r})/\lambda}\right]/r^2\right\}\rho'(r) \\ &= \left(B_0^{m+1}/m!\right)\left(r - R_0\right)^m \mathrm{e}^{-B_0(r-R_0)} \qquad (r \geqslant R_0) \\ &= 0 \qquad\qquad (r < R_0). \end{aligned} \tag{2}$$

Here $m = 0, 1, 2$; B_0 is a disorder parameter. The centroid of this distribution or the mean distance $\bar{r} = R_0 + (m+1)/B_0^2$. The convolution of this model with Gaussian function P_G (i.e., $P_G(r) \otimes P^m(r)$, which will be referred to as MD3), as a softening model for the repulsive potential, is effective for obtaining the thermal motion of atoms and static structure disorder with a broadening of the peak in the distribution. The relevant function form used to simulate the experimental data is

$$\chi(k) = N'B(k)\left(1 + z^2\right)^{-(m+1)/2} \mathrm{e}^{-2k\sigma_G^2} \sin\left[2k\bar{r} + (m+1)\left(-z + \tan^{-1} z\right) + \delta(k)\right] \tag{3}$$

where $z = 2k/B_0$; N' is an *effective* coordination number. The normalized real RDF is $\rho(r) = (1/Z)\rho'(r)$, where Z is a normalized constant; the real coordination number $N = N' \int_0^{+\infty} \rho'(r)\mathrm{d}r$.

(iii) *Discrete probability distribution model (MD4).* Define the effective RDF as [18, 20]

$$P(r) = \left\{\left[\mathrm{e}^{-2(r-r_p)}/\lambda\right]/r^2\right\}\rho'(r) = (1/Z)\exp\left[-y^2/2\sigma^2\right] \tag{4}$$

where $y = (r - r_p)\exp[-a(r - r_p)]$; r_p is the peak position of the distribution; a is an asymmetric parameter. The spectrum for one shell is simulated using the following function:

$$\chi(k) = \sum_{j=1}^{9} N' P_j B(k) \sin\left[2kr_j + \delta(k)\right] \tag{5}$$

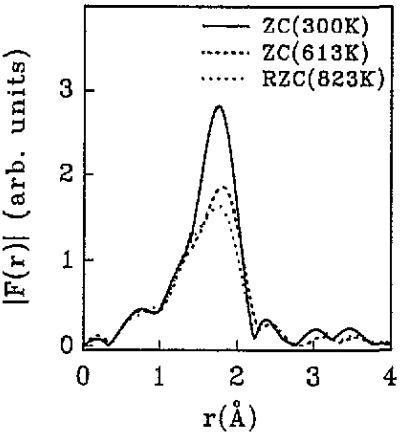

Figure 1. The magnitudes of the Fourier transform of $k^3\chi(k)$ (Zn K edge) for $ZnCl_2$ (ZC) and Rb_2ZnCl_4 (RZC) at varying temperatures.

where

$$P_j \equiv P(r)\Delta r = (1/\sqrt{4\pi})e^{-(j-5)^2/4}$$

$$r_j = \left[(\sigma^2/2)^{1/2}(j-5)\right]e^{a(\sigma^2/2)^{1/2}(j-5)} + r_p$$

$j = 1, 2, \ldots, 9$. The RDF is $\rho(r) = (1/Z)P(r)$, $\bar{r} \simeq (1/Z)\sum_{j=1}^{9} r_j H_j$ and $N \simeq N' \sum_{j=1}^{9} H_j$; here $H_j = r_j^2 e^{2(r_j - r_p)/\lambda} P_j$; Z is also a normalized constant.

For each model mentioned above, the backscattering amplitude $B(k)$ and the phase shift $\delta(k)$ can be extracted from the literature. In practice, the energy difference ΔE_0 is added as a fitting parameter. For the spectra taken at different temperatures for the three samples $ZnCl_2$, RbCl and Rb_2ZnCl_4 we subtracted the pre-edge background by fitting pre-edge data with the Victoreen formula. They were converted to k space using the formula $k = [2m(E - E_0)]^{1/2}/\hbar$ by setting E_0 at a half of the absorption jump. $\chi(k)$ was obtained with the equation $\chi(k) = [\mu(k) - \mu_0(k)]/\Delta\mu_0$, where $\mu_0(k)$ is a cubic spline curve best fitting average behaviour of $\mu(k)$ above the absorption edge; $\Delta\mu_0$ is the edge jump.

3.1. Zn–Cl shell

The fast Fourier transform of $k^3\chi(k)$ was calculated in the k range 2.49–11.35 $Å^{-1}$ for the Zn K-edge absorption spectra; during the transform a Hanning window function as described by Sayers and co-workers [18] was used with the parameter $F \simeq 0.2$. The Fourier transform magnitudes for $ZnCl_2$ and Rb_2ZnCl_4 at different temperatures are shown in figure 1. It is obvious that for the molten $ZnCl_2$, the main peak of the first-neighbour shell about Zn is slightly shifted to large r and the peak height decreases relative to that of the solid state at the room temperature. The local structures around the Zn atoms in the two melts are also compared in figure 1. It should be noted that even in the two different melts, the local structures around the Zn atoms are similar just above their melting points. The back Fourier transform was carried out with a range from 0.92 Å to 2.35 Å, and a Hanning window with $F \simeq 0.2$ was also used. The filtered function $k^3\chi_1(k)$ from the Zn–Cl single-shell contribution to EXAFS was then obtained.

At room temperature there are 4 Cl neighbours to Zn with mean distance 2.273 Å for $ZnCl_2$ [22] and it is reasonable to take this as a reference with the Gaussian model to obtain the RDFs of the two melts. The value of σ_r^2 was calculated using the FEFF408 program [23], and λ could also be estimated from the calculations. The backscattering amplitude and phase shift of the Zn–Cl atom pair were extracted from the $k^3\chi_1(k)$ function.

MD4 has been used to achieve RDFs of the melts. In (5), there are five parameters can be given by simulation: they are N', r_p, σ^2, a and ΔE_0. For $a = 0$ the effective distribution is Gaussian, $a > 0$, skews the distribution on the large-r side, and $a < 0$ skews it in the small-r side. However, this model has its limitations: besides the common problems in curve fitting, it is found that the results are reasonable only for small values of a, and it is difficult to give a quantitative interpretation of the parameter a describing the real disorder. On the other hand, using this effective method, we can obtain reasonable results with an acceptable accuracy as tabulated in table 1. Q is a factor describing the goodness of fit, defined as $[\sum_i(\chi_i^{fit} - \chi_i^{exp})^2]^{1/2}/[\sum_i(\chi_i^{exp})^2]^{1/2}$, where χ_i^{exp} denotes the experimental data and χ_i^{fit} the fitting data. The error bars in table 1 were obtained by analysing separately different scans under the same experimental situation. They include the deviation resulting from the experimental procedure and data analysis (e.g., the different isolation window sizes and different fitting ranges). The normalized RDFs can easily be obtained. One can find from figure 2 that the distributions of the nearest-neighbour Cl atoms around Zn atoms in the melts are broader than that in the solid $ZnCl_2$ and the functions present little asymmetry.

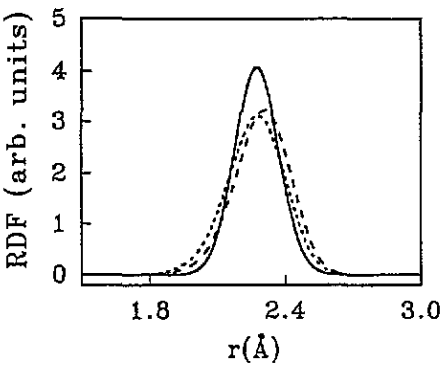

Figure 2. The normalized RDFs for the nearest-neighbour atoms (Cl) around Zn in $ZnCl_2$ at 300 K (solid line) and 613 K (long-dashed line) and Rb_2ZnCl_4 at 823 K (short-dashed line) obtained from model-dependent method MD4.

3.2. Rb–Cl shell

The first step to isolate the Rb–Cl shell EXAFS function is similar to that for the Zn–Cl shell; here the transform from k to r space is over the range 2.1–11.1 $Å^{-1}$. The magnitudes of Fourier transforms for RbCl and Rb_2ZnCl_4 melts are plotted in figure 3. It should be pointed out that there is a peak with relatively strong intensity at small r in each magnitude (not plotted in the figure, to stress the local structure around Rb), which has been recognized as a product from multielectron excitation [24]. Such a peak could be completely removed if the μ_0 curve was *forced* to pass through the step in the absorption spectra (the position is about

Table 1. Structural parameters for the nearest-neighbour shell of Cl atoms around Zn in the molten salts $ZnCl_2$ (ZC) and Rb_2ZnCl_4 (RZC). The data are obtained using a model-dependent method (MD4). Q is a factor describing the goodness of fit.

		300 K		613 K (ZC), 823 K (RZC)				
Method	Sample	N	R (Å)	N	R (Å)	σ^2 ($\times 10^{-2}$ Å^2)	a (Å^{-1})	Q
MD4	ZC	—	—	4.3±0.2	2.31±0.01	1.7±0.1	−0.23±0.09	0.10
	RZC	—	—	4.2±0.2	2.28±0.01	1.8±0.1	−0.21±0.08	0.11
	ZC	4.0 [22]	2.27 [22]	3.9 [3]	2.29 [3]	—	—	—
	RZC	4.0 [12]	2.24 [12]	—	—	—	—	—

135 eV above the edge), but it is argued that the result is unreliable because the artificially distorted μ_0 obscures the meaningful information about the Rb–Cl shell, especially for a large disordered melt with relatively weak EXAFS intensity. Fortunately, the spurious peak at about 0.9 Å is far from the peak of interest, so there is no harm in retaining it. For molten RbCl, figure 3 shows that the first peak of Rb–Cl reduces and shifts to small r relative to the solid. Such a large reduction is due to very strong disorder, which results in significant asymmetry in distribution. In figure 3(b), the comparison between the molten RbCl and Rb_2ZnCl_4 shows that the asymmetric degrees of Rb–Cl distributions are different in the two melts. The back Fourier transform was taken in the range 1.8 Å$< r <$ 3.1 Å with a window function as mentioned previously.

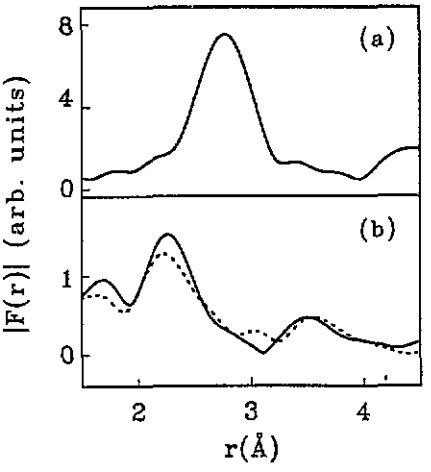

Figure 3. The magnitudes of the Fourier transforms of $k^3\chi(k)$ (Rb, K edge) for (a) RbCl at 80 K, (b) RbCl at 1023 K (solid line) and Rb_2ZnCl_4 at 823 K (dashed line).

The next step is to obtain the RDFs of the melts. The structure of the RbCl crystal is NaCl type with 6 Cl neighbours to Rb at 3.291 Å [25]. The spectrum of RbCl at 80 K was taken as a reference to analyse the Rb-edge data. The values of σ^2 and λ were also calculated theoretically using the FEFF program, so the RDF of RbCl at 80 K could be easily constructed, as shown in figure 4(a). Model-dependent methods were applied and

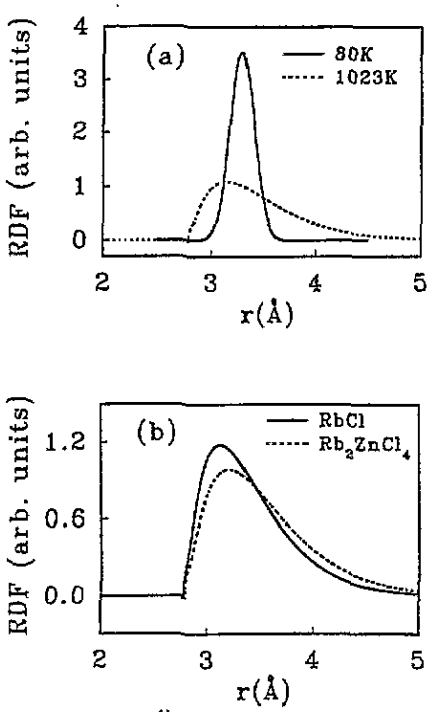

Figure 4. (a) The normalized RDFs of the nearest-neighbour atoms (Cl) around Rb in solid *80 K) and liquid RbCl (1023 K). (b) The RDFs of the first shell around Rb in molten RbCl (1023 K) and Rb_2ZnCl_4 (823 K) are compared.

some models, such as MD1, MD2, MD3 (m = 0) and MD4, were tried in turn by fitting the experimental curve $k^3\chi_1(k)$ over the range 2.1–11.1 Å^{-1}, but for the first three models, the results were unreasonable and unacceptable; for the last one the fitting procedure was simply difficult to continue even though varying the initial parameters. On the other hand, the model MD3 (m = 1), i.e., $p^1(r) \otimes G(r)$ was then applied and found to be appropriate for obtaining the RDFs of the two melts; it gave the structural parameters with tolerable goodness of fit (assuming the Rb atom penetration into the first shell is very small and can be neglected). In table 2, $C_2 = \sigma^2 + 2/B_0^2$, which reflects the degree of disorder in the sample; the error bars in the table are calculated as previously but with somewhat larger values, which are due to the relatively large error owing to the poor signal-to-noise ratio for the spectra of the melts. The normalized RDFs of the two melts were then obtained as presented in figure 4. It can be noted from table 2 that there are 4.8±0.9 Cl atoms at a mean distance 3.28±0.07 Å in the Rb–Cl shell for the molten RbCl and 7.6±0.6 Cl atoms at a distance 3.41±0.04 Å for the molten Rb_2ZnCl_4. Figure 4(a) indicates that in the first shell the Cl atoms have a rather wider distance distribution in the RbCl melt than in its solid. Figure 4(b) compares the RDFs of the two different melts; it is found that for Rb_2ZnCl_4 the range of distance distribution is slightly larger than that for RbCl, which is also reflected in the difference between their values of $\sigma^2 + 2/B_0^2$.

It should be pointed out that the RDF obtained from EXAFS data is mainly the RDF of the first-nearest-neighbour atoms around the absorption atom. For larger disordered systems, the second- and higher-nearest neighbours make a measurable contribution to the full EXAFS only in the low-k region [18]. The information about these atoms is almost lost owing to the lower limit $k_{min} \sim 2$ Å^{-1} in the data analysis presented here, so the RDF obtained from

Table 2. Best-fit parameters for the first-neighbour shell of Cl atoms around Rb in the molten RbCl (RC) and Rb_2ZnCl_4 (RZC) using the model $P^1(r) \otimes G(r)$ (MD3). Here $C_2 = \sigma^2 + 2/B_0^2$. Q is a factor describing the goodness of fit.

		300 K		1023 K (RC), 823 K (RZC)					
Method	Sample	R N	(Å)	R N	σ^2 (Å)	B_0 ($\times 10^{-3}$ Å^2)	C_2 (Å^{-1})	($\times 10^{-2}$ Å^2)	Q
MD3	RC	—	—	4.8±0.9	3.28±0.07	2.9±1.0	4.2±0.7	1.2±0.3	0.17
	RZC	—	—	7.6±0.6	3.41±0.04	5.7±0.3	3.3±0.2	1.9±0.2	0.20
	RC	6.0 [25]	3.29 [25]	6.9 [8]	3.18 [8]	—	—	—	—
	RZC	7.5 [12]	3.52 [12]	—	—	—	—	—	—

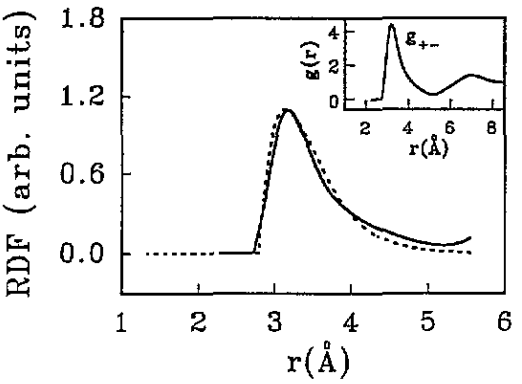

Figure 5. The normalized RDFs of the nearest-neighbour atoms (Cl) around Rb in molten RbCl obtained from neutron scattering (solid line) and EXAFS (dashed line) are compared. The RDF of the neutron experiment as shown in the inset is quoted from [8].

EXAFS data is only loosely related to the function $g_{+-}(r)$ determined from neutron diffraction with isotopic substitution. Figure 5 shows the difference between the two normalized RDFs obtained with neutron [8] and EXAFS experiments.

4. Discussion and conclusions

The structures of molten $ZnCl_2$, RbCl and Rb_2ZnCl_4 have been studied using EXAFS technique. Some RDFs of these compounds in the solid and liquid states are obtained with model-dependent methods. For molten $ZnCl_2$, the model-dependent method with discrete probability distribution is appropriate, and we find the first-neighbour shell around Zn has 4.3±0.2 Cl atoms at a mean distance of 2.31±0.01 Å, whereas the coordination number and the bond length obtained from the neutron scattering experiment [6] are 3.9±0.1 and 2.29±0.01 Å, respectively. The RDF (figure 2) presents little asymmetry and slight broadening, which indicates that either the local structures around Zn atoms are very stable or the short-range order in the solid state persists just above its melting point. Considering the atomic-thermal motion, the result implies the Cl atoms are in slow exchange among the $(ZnCl_4)^{2-}$ and other complexes or, as described by Enderby and Barnes [26], the complexes themselves undergo cooperative motion, which is also consistent with the differences in

properties from other 2:1 molten salts, e.g., its particularly small self-diffusion coefficient and low electrical conductivity.

The model-dependent ($P'(r) \otimes G(r)$) has been applied to determine the local structure for molten RbCl and the results have been confirmed by comparison with those from the other attempts. To our surprise, the disorder in the melt is so large that the peak from the Rb–Cl contribution in the Fourier transform magnitude is very weak, which is also one of the origins of error in the results. On average there are 4.8±0.9 Cl neighbours for each Rb, which is smaller than the value of 6.9 from neutron experiments [8]. This disagreement is fair and reasonable for such a large disordered system, because the EXAFS data analysis was restricted to the range 2.1 $\text{Å}^{-1} < k < 11.1\ \text{Å}^{-1}$; as described in section 3, the lack of the low-k contribution has led us to miss the information on a few atoms at larger nearest-neighbour distances from the absorption atom. From figure 5 the Cl atoms are found in the first-neighbour shell around Rb with a distance distribution range from 2.8 Å to 4.5 Å, as well as the RDF having significant asymmetry behaviour. Considering that the mean distance is about 3.28 Å, the density of solid RbCl is 2.80 g cm^{-3} and that of the liquid 2.09 g cm^{-3}, the following semi-empirical formula [26] is well satisfied by our results:

$$n_l^{+-} = n_s^{+-}(V_s/V_l)(\bar{r}_l^{+-}/\bar{r}_s^{+-}) \tag{6}$$

where V_l and V_s are the molar volumes of the liquid and solid states, which can be calculated from their density values; n_s^{+-} and $\bar{r}_s^{+-}$ are structure parameters for Rb–Cl coordination in the solid state; $\bar{r}_l^{+-} = 3.28 \pm 0.07$ Å from our results. n_l^{+-}, which is the nearest-neighbour number of Cl atoms around Rb in the liquid state, is about 4.4 obtained from (6); this is very near 4.8 determined here. The fact that (6) is satisfied implies that the short-range order in molten RbCl is similar to that of the solid, but the disorder is larger, which is due to the high mobility of Rb^+ and Cl^- atoms. It should be pointed out that because of a small amount of Rb moving into the first-neighbour shell, and in addition the non-transferability of the phase shift and backscattering amplitude (even though we are only interested in the first shell and take ΔE_0 as a fitting parameter), due to the large distance distribution, the quantitative results for the melt are only average ones and not very accurate, but are adequate to gain valuable structural information.

For molten Rb_2ZnCl_4, the local structures around Zn and Rb have been investigated using the same methods as for molten $ZnCl_2$ and RbCl, respectively. Table 1 indicates there are 4.2±0.2 Cl atoms around Zn in the melt at a slightly larger mean distance, 2.28±0.01 Å, than that in the solid Rb_2ZnCl_4. The increase in distance is due to thermal expansion, similar to that in molten $ZnCl_2$. Figure 2 shows that the RDF of molten Rb_2ZnCl_4 has almost no asymmetry but has some differences from that of molten $ZnCl_2$, such as the deviations between their maximum positions and their different asymmetries (even though these are small) and distribution ranges, which suggest that the environments around the $ZnCl_4$ groups in the melts Rb_2ZnCl_4 are not the same as those in molten $ZnCl_2$, which contains tetrahedral units linked via corner sharing of Cl ions to form a network. A reasonable situation is that the network does not exist in molten Rb_2ZnCl_4, i.e., the $ZnCl_4$ is isolated as in solid Rb_2ZnCl_4 and also very stable in the liquid state.

Table 2 gives the local structural parameters around Rb in molten Rb_2ZnCl_4: there are 7.6±0.6 Cl atoms neighbouring with Rb and the degree of short-range disorder is even larger than that in molten RbCl because of the smaller value of disorder parameter B_0 (4.2±0.7 Å^{-1} for RbCl and 3.3±0.2 Å^{-1} for Rb_2ZnCl_4). This is also indicated in figure 4(b) by comparing their RDFs. The two distribution patterns are similar but the RDF of Rb_2ZnCl_4 is slightly

shifted to large r (the mean distance is 3.41±0.04 Å) without too steep a leading edge but with a small increase in the large-r side relative to that of molten RbCl. It can therefore be regarded that the average coordination number results from solid-state Rb_2ZnCl_4 (Rb(1)–8Cl, Rb(2)–9Cl), and not from molten RbCl, taking account of a reasonable reduction by the mobility of ions in the melt.

It can be concluded that the Zn–4Cl coordination exists in the form of the isolated $ZnCl_4$ complexes and that these are relatively stable or have small disorder in themselves, but Rb atoms with larger mobility among these complexes have, at any rate, larger disordered local structures with neighbouring Cl atoms (possibly a small amount of penetration of Zn is negligible during data analysis, which would mainly affect the goodness of fit). It is interesting that these characteristics of the local structure in the melt can also be found, to some extent, in the crystalline Rb_2ZnCl_4, e.g., Rb atoms have very large disordered environments. Knowing the relation between the structures of a melt and the corresponding crystal is without doubt significant for our understanding of the structural unit and the mechanisms of crystal growth. The results here are consistent with that of Allen *et al* [11], considering the molten Rb_2ZnCl_4 as a mixture of the two melts $ZnCl_2$ and RbCl, and RbCl can be regarded as a network breaker.

Furthermore, the skewed shape of the RDF (figure 4) enables us to substitute the excluded-volume model [19] for the microscopic potential of the ion–ion pair interaction, in which a softened 'hard-sphere' repulsive potential was used. The steep leading edge of the RDF here also indicates that the core–core repulsion between the Rb^+ and Cl^- must be rather strong, which will be helpful in specifying and selecting the model potentials in our further work of studying the molten Rb_2ZnCl_4 using molecular dynamics.

Acknowledgments

We would like to thank Professor Xiao Nan, Professor Li Chenxi and Wang Yuren for their assistance with the experiments. We wish to thank both the Photon Factory of Japan and Synchrotron Radiation Laboratory in Beijing. We are also grateful to Dr Nomura, Xie Yaning, Huang Daxian, Hu Tiantuo, Qiao Shan and Hai Yang for help during the EXAFS measurements. This work is supported by the Chinese National Science Foundation and a grant for a key research project in the Climbing Programme from the State Science and Technology Commission of China.

References

[1] Triolo R and Narten A H 1981 *J. Chem. Phys.* **74** 703
[2] Biggin S and Enderby J E 1981 *J. Phys. C: Solid State Phys.* **14** 3577
[3] Woodcock L V, Angell C A and Cheeseman P 1976 *J. Chem. Phys.* **65** 1565
[4] Gardner P J and Heyes D M 1985 *Physica* B **131** 227
[5] Kumta P N, Deymier P A and Risbud S H 1988 *Physica* B **153** 85
[6] Allen D A, Howe R A and Wood N D 1991 *J. Chem. Phys.* **94** 5071
[7] Wong J and Lytle F W 1980 *J. Non-Cryst. Solids* **37** 273
[8] Mitchell E W J, Poncet P F and Stewart R J 1976 *Phil. Mag.* **34** 721
[9] Dixon M and Sangster M J L 1977 **35** 1049
[10] Ellis R B 1966 *J. Electrochem. Soc.* **113** 485
[11] Allen D A, Howe R A, Wood N D and Howells W S 1992 *J. Phys.: Condens. Matter* **4** 1407
[12] Secco A S and Trotter J 1983 *Acta Crystallogr.* C **39** 317
[13] Quilichini M and Pannatier J 1983 *Acta Crystallogr.* B **39** 657

[14] Itoh K, Hinisada A A, Matsunaga H and Nakamura E 1983 *J. Phys. Soc. Japan* **52** 664
[15] Lu H M and Hardy J R 1992 *Phys. Rev.* B **45** 7609
[16] Hayes T M and Boyce J B 1980 *J. Phys. C: Solid State Phys.* **13** L731
[17] Bunker G 1983 *Nucl. Instrum. Methods* **207** 437
[18] Sayers D E, Bunker B A, Crozier E D, Rehr J J and Ingalls R 1988 *X-ray Absorption: Principles, Applications and Techniques of EXAFS, SEXAFS and XANES* ed D C Koningsberger and R Prins (New York: Wiley) pp 221, 373
[19] Boyce J B, Hayes T M and Mikkelsen J C 1981 *Phys. Rev.* B **23** 2876
[20] Alberding N and Crozier E D 1983 *Phys. Rev.* B **27** 3374
[21] Stern E A, Ma Y, Petitpierre O H and Bouldin C E 1992 *Phys. Rev.* B **46** 687
[22] Yakel H L and Brynestad J 1978 *Inorg. Chem.* **17** 3294
[23] Mustre de Leon J, Rehr J J, Zabinsky S I and Albers R C 1991 *Phys. Rev.* B **44** 4146
[24] Li G G, Bridges F and Brown G S 1992 *Phys. Rev. Lett.* **68** 1609
[25] Swanson *et al* 1953 *NBS Circular 539* 4 41
[26] Enderby J E and Barnes A C 1990 *Rep. Prog. Phys.* **53** 85